We are IntechOpen,
the world's leading publisher of
Open Access books
Built by scientists, for scientists

6,900
Open access books available

186,000
International authors and editors

200M
Downloads

154
Countries delivered to

Our authors are among the

TOP 1%
most cited scientists

12.2%
Contributors from top 500 universities

CLARIVATE ANALYTICS
BOOK CITATION INDEX
INDEXED

WEB OF SCIENCE™

Selection of our books indexed in the Book Citation Index
in Web of Science™ Core Collection (BKCI)

Interested in publishing with us?
Contact book.department@intechopen.com

Numbers displayed above are based on latest data collected.
For more information visit www.intechopen.com

Methodology for the Assessment of Joint Efforts During Sit to Stand Movement

Maxime Raison, Maria Laitenberger, Aurelie Sarcher, Christine Detrembleur, Jean-Claude Samin and Paul Fisette

Additional information is available at the end of the chapter

http://dx.doi.org/10.5772/49996

1. Introduction

The sit to stand (STS) analysis and particularly the 5-repetition sit-to-stand test (FRSTST) introduced by Bohannon [1] are widely used measurements of functional strength and disability level of young and elderly subjects. For example in rehabilitation and orthopedics, these tests are mainly used for the functional evaluation of :

- children with cerebral palsy, for which the FRSTST was found a reliable and valid test to measure functional muscle strength in children with spastic diplegia in clinics [2, 3];
- older adults, for which the FRSTST test-retest reliability can be interpreted as good to high in most populations and settings [1];
- subjects with Parkinson's disease [4];
- paraplegic subjects [5];
- subjects with multiple sclerosis [6];
- above knee amputees [7] and unilateral transtibial amputees [8];
- subjects with rheumatoid arthritis [9] or alterations in advanced knee osteoarthritis [10];
- post-stroke subjects [11].

The STS analysis also currently helps to develop :

- STS assistive device for the elderly and disabled [12];
- STS and gait support system for elderly and disabled [13], and also handrail positions and shapes that best facilitate STS movement [14];
- car cockpits taking into account the comfort analyzes of subject seated in a car [15, 16] or on a simple seat [17, 18].

Usually, the functional strength and the disability level during STS are evaluated by calculating the total forces of hip and knee extensors [1] and the center of mass (COM) accelerations [19]. Nevertheless, it is known that determining with accuracy the kinematics (including the COM) and dynamics (including the joint forces and torques) in the human body is still a great challenge in biomechanical modeling [20]. Consequently, the aim of the present study consists in presenting a rigorous methodology for the non-invasive assessment of joint efforts and the associated kinematic variables during STS movement. This method is based on a three-dimensional dynamical inverse model of the human body. Like other classical *dynamical inverse* analyzes [21–25] in biomechanics of motion, the model proposed here [18] uses measurements of external interactions (forces $\mathbf{F}_{ext}$ and torques $\mathbf{M}_{ext}$) between the body and its environment, and also measurements of the system configuration x_{exp}. The corresponding joint coordinates q are numerically determined by a kinematic identification process, and the corresponding velocities $\dot{q}$ and accelerations $\ddot{q}$ are presently estimated from the q, using a numerical derivative. Finally, the model provides the joint interactions with the use of a symbolically generated recursive Newton-Euler formalism [26, 27].
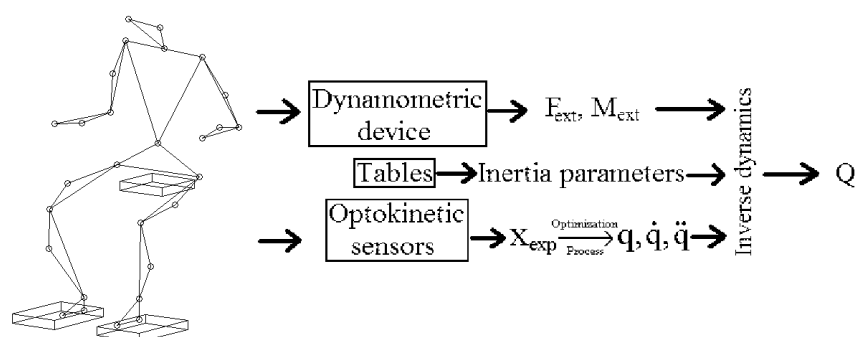

Figure 1. Principle of the inverse dynamical model: from the experiment to the vector Q of the joint efforts.

This model is applied to experiments of STS : the subject, initially seated, is asked to get up without moving the feet, and without arm or hand contact with the environment or with any part of the body. In this paper, both postural behaviors of slow and fast STS are analyzed and compared.

2. Material and methods

First, this section summarizes the features of the proposed human body model and describes the corresponding experimental set-up and process. Second, a preliminary calculation defines the centers of mass and centers of pressure of the model, and also develops the relation between their local and global components: these variables are known as diagnostic tools in rehabilitation and physical ergonomics [28–30], and useful for the present model analysis. Third, the theoretical investigation will develop both kinematic and dynamical analyzes related to this model, and both analyzes will be applied to the STS.

2.1. Model features and hypotheses

The proposed human body model is composed of 28 position sensors (Fig. 2), defining 13 rigid bodies: the head, both upper arms, both lower arms, the trunk, the pelvis, both thighs, both shanks, and both feet. Each of the 13 bodies is defined by three position sensors, in order to

know the three-dimensional configuration of each body. Further, these bodies are linked by spherical joints corresponding to 12 anatomical landmarks (referring to [31]): the C7 vertebra, both shoulders (acromioclavicular joints), both elbow joint centers, the sacrum, both greater trochanters, both knee joint centers, both lateral heads of the malleolus. Consequently, the system is fully described by a total of *13 (bodies) × 6 variables - 12 × 3 spherical joint constraints = 42 generalized coordinates*, representing the 42 degrees of freedom of the model. As shown in Fig. 1, the inverse dynamical model provides the column vector Q of joint forces and torques, using three sets of inputs:

1. The external forces and torques.

2. The inertia parameters.

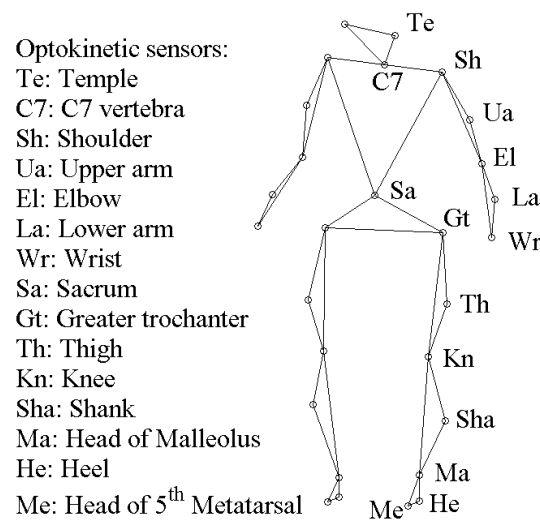3. The joint coordinates, velocities and accelerations.

Figure 2. Human body model, featuring the 28 optokinetic sensors that define the 13 articulated rigid bodies, each defined by three points, articulated via 12 spherical joints.

A few characteristics and assumptions must be formulated about these three sets of inputs:

- The external forces $\mathbf{F}_{ext}$ and torques $\mathbf{M}_{ext}$ between the body and its environment are measured by a dynamometric device. The external pure torques are not considered.

- The body inertia parameters, i.e. the masses m_i, moments of inertia I_i and center of mass positions $\overrightarrow{OM_i}$ of the ith body member (i = 1,...,13) are taken from the inertia tables of de Leva [31] (1996) readjusted from the Zatsiorsky-Seluyanov's mass inertia parameters [32] (1990). The inertia parameter identification is not part of this research: indeed, previous investigations [33] showed that non-invasive in-vivo identifications of the body parameters are presently inappropriate to the human body dynamics, because the resulting body parameters have significant errors due to experimental errors in the input data, such as the body configuration, or the external force and torque measurements.

- The system configuration, i.e. the experimental absolute coordinates x_{exp} of the reference points, are measured by the 28 optokinetic sensors. The corresponding joint coordinates q are numerically determined by a kinematic identification process and the corresponding velocities $\dot{q}$ and accelerations $\ddot{q}$ are presently estimated from the q by a numerical derivative

using finite differences. Considering the joint kinematics, we are aware that more adequate joint models could be used: in particular, previous studies [34, 35] have developed more complex three-dimensional joints for the knee and the shoulder. The present model has been implemented with spherical joints but will be extended to include more involved joints in the future. Further, the results of the kinematic analysis for this experiment show that the spherical joints considered here sufficiently fit the considered motion (see Section 3.1).

2.2. Experimental set-up and procedure

Let us consider the system reference frame $[\hat{I}]$, located at a fixed point O on the laboratory floor (Fig. 3). In this reference frame, the motion measurement set-up consists of optokinetic sensors and six infra-red cameras ($Elite - BTS^{TM}$), that estimate the coordinate vectors $\overrightarrow{OX}_{exp,n} = [\hat{I}]^{\top} x_{exp,n}$) of the joint reference points, i.e. of the optokinetic sensors. Further, the interaction measurement set-up consists of two force platforms at the feet contact and one force platform at the seat, for the determination of the horizontal and vertical interaction forces $\mathbf{F}_{ext} = [\hat{I}]^{\top} F_{ext}$ and torques $\mathbf{M}_{ext} = [\hat{I}]^{\top} M_{ext}$ between the body and these platforms. The three independent platforms are composed of four force sensors [36], designed by our laboratory, and located at the edges of these platforms. The device provides a total number of *3 platforms × 4 force sensors × 3 force components = 36 force components*. All data are sampled at 100 Hz, using an adaptive low-pass numerical filter (implemented by $Elite - BTS^{TM}$).

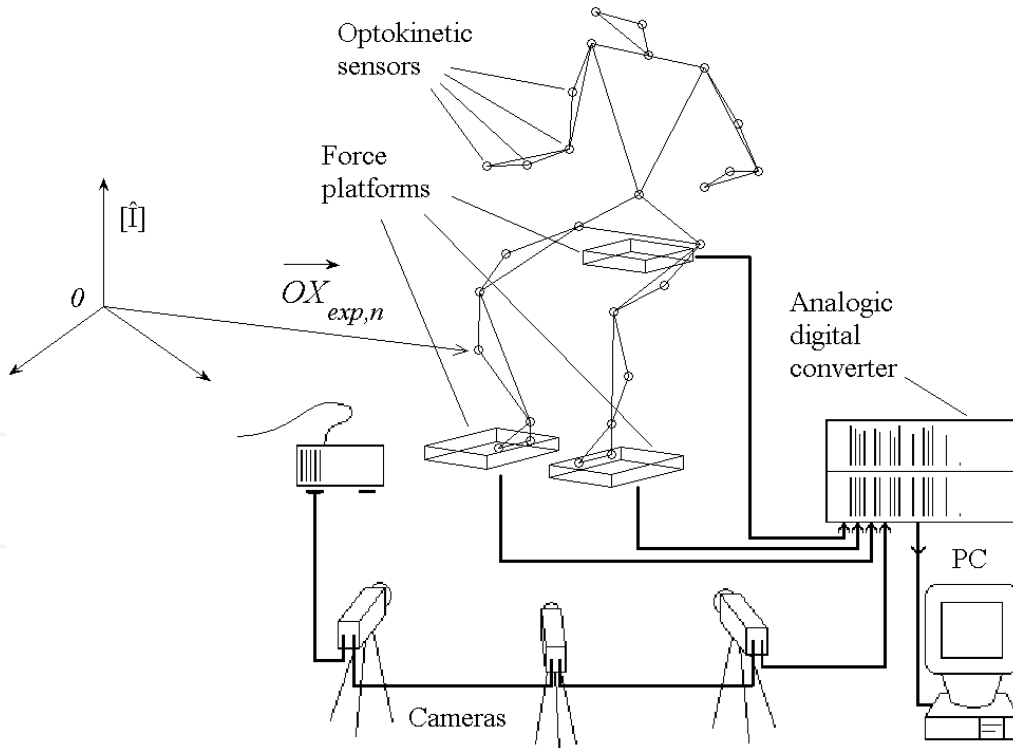**Figure 3.** Experimental set-up, related to the system reference frame $[\hat{I}]$, located at a fixed point O on the laboratory floor. $\overrightarrow{OX}_{exp,n}$ represents the coordinate vectors of the optokinetic sensors.

The experiments were performed by one person related to our laboratory, who gave his informed consent to perform the experiments. Note that further experiments of STS are

presently performed in order to discuss the repeatability of the data and results for several subjects and several behaviors of STS.

At the beginning of each test, the subject is seated as shown in Fig. 3. Then the subject is asked to get up from the seat. During the whole experiment, the observers check that:

- the subject do not move feet, in order to obtain a good repeatability of the initial and final body configurations;
- the subject has neither arm nor hand contact with the environment or the rest of the body.

Two behaviors of STS are analyzed and compared in this paper, in order to compare a "slow" and a "fast" STS. For both tests, the time evolution of the body motion permits the definition of three phases:

1. The initial phase: the subject is seated, it is assumed that the subject is at an equilibrium state, i.e. the subject is only performing forces necessary to maintain his initial posture.
2. The transient phase, composed of two sub-phases: a first transient sub-phase when the subject begins to get up and the subject thighs are still in contact with the seat; a second transient sub-phase, when the subject continues to get up without seat contact.
3. The final phase: the subject maintains his standing-up position; it is assumed that this is the second equilibrium state of the subject during the test.

2.3. Center of mass and center of pressure

This section defines the centers of mass and centers of pressure of the proposed model, and also develops the relation between their local and global components [29, 30].

2.3.1. Centers of mass

The position of the *global center of mass* (GCOM) of the human body can be written as follows:

$$\overrightarrow{OM} = \frac{\sum_{i=1}^{13} m_i \overrightarrow{OM_i}}{\sum_{i=1}^{13} m_i} \tag{1}$$

where

- $\overrightarrow{OM_i}$ is the position vector of the *local center of mass* LCOM of the ith body member (i=1,...,13); the values of $\overrightarrow{OM_i}$ are estimated from the human body configuration and the inertia tables of de Leva [31];
- m_i is the mass of the ith member (i=1,...,13); the values of m_i are estimated from the inertia tables.

Remember that the integration of the platform force data provides more accurate values of the GCOM variations [37], which are used as diagnostic tools in rehabilitation and physical ergonomics. However, the GCOM calculated by this method is equal to the actual GCOM plus one undetermined constant value. Further, it was shown for instance that the differences

between the GCOM estimated by these two methods are less than 0.3% height in all 3 components for able bodied subjects [37]. Consequently, the upper definition of the GCOM is preferred to estimate the actual GCOM value of the present human body model.

2.3.2. Centers of pressure

For each force platform, the *local center of pressure* (LCOP) components, related to the system referential point O, can be determined from the platform force data, using the following definition:

$$\overrightarrow{OP}_j = (X_{P_j}, Y_{P_j}, Z_{P_j}) = \left(-\frac{M_{Y_j}}{R_{P_{j,z}}}, \frac{M_{X_j}}{R_{P_{j,z}}}, H_j \right) \tag{2}$$

where

- the index j indicates the platform: j = 1, 2 or 3 for the left foot platform, the right foot platform or the seat platform, respectively;

- $R_{P_{j,z}}$ is the vertical component of the force on the jth platform;

- M_{X_j} and M_{Y_j} are anterior-posterior and lateral components, respectively, of the resulting moment on the jth platform, related to the reference O;

- H_j is the measured height of the jth platform; H_j is the assumed to be constant during the experiment.

The *global center of pressure* (GCOP) [29, 30] is defined as the weighted sum of the LCOP on every contact platform. Its expression related to the system referential point O is given by :

$$\overrightarrow{OP} = \frac{\sum_{j=1}^{3} R_{P_j} \cdot \overrightarrow{OP}_j}{\sum_{j=1}^{3} R_{P_j}} \tag{3}$$

where, for the platforms from j = 1 to 3 (i.e. j = 1 for the left foot platform, j = 2 for the right foot platform and j = 3 for the seat platform) :

- the index j indicates the platform;

- $\overrightarrow{OP}_j$ is the vector of position of the LCOP on the jth platform;

- R_{P_j} is the global force data on the jth platform.

Let us note that $\overrightarrow{OP}_i$ and R_{P_j} are totally estimated from the platform force data. In particular, during the second part of the transient phase and the final phase, when there is no contact between the subject thighs and the seat, $R_{P_3} = 0$ and $\overrightarrow{OP}$ does not take into consideration OP_3, which is undetermined from Equation (2).

Finally, both centers of mass and centers of pressure will be presented in the 'Results' Section, because these are useful in rehabilitation and physical ergonomics. However, only the LCOMs, estimated from the system configuration and the tables of inertia, are essential for the implementation of the musculoskeletal analysis presented in Fig. 1.

2.4. Theoretical investigation

The theoretical investigation of the model is developed in two steps :
- First, the joint coordinates q are numerically determined by an identification process that estimates the joint coordinates of the multibody model that best fit the experimental joint positions $x_{exp,n}$.
- Second, the dynamical model provides the vector Q of joint torques during the experiments, using a symbolic generated recursive Newton-Euler formalism. Let us note that this vectorial formulation allows the results to be independent of the angle variable in the spherical joints, whose choice and sequence are rather defined for a methodical implementation than for physiological reasons.

2.4.1. Kinematic analysis

The joint coordinates q are numerically determined by an identification process that estimates the joint coordinates of the multibody model that best fit the experimental joint positions $x_{exp,n}$. As proposed by Ref. [20], the optimization problem can be formulated as a nonlinear least-square problem applied for each body configuration, at each time instant t_k, $k = 1, \ldots, T$, where T is the last time sample of each test. Consequently, the cost function $f_{cost}(t_k)$ can be written at each time instant t_k as follows:

$$f_{cost}(t_k) = \sum_{n=1}^{28} |x_{mod,n}(q(t_k)) - x_{exp,n}(t_k)|^2 \tag{4}$$

where

- the index $n = 1, \ldots, 28$ indicates the optokinetic sensor;

- $q(t_k)$ is the joint coordinate vector at the time instant t_k, and is the variable of the optimization process;

- $x_{mod,n}(q(t_k))$ is the cartesian coordinate of the nth optokinetic sensor at the time instant t_k, obtained from the $q(t_k)$, using the forward kinematic model;

- $x_{exp,n}(t_k)$ is the cartesian coordinate of the nth optokinetic sensor at the time instant t_k, provided by the experimental set-up.

Fig. 4 schematically outlines the identification process, which involves two consecutive steps:

1. A pre-process calculates the mean distances l_i between the joints for each of the ith body member, using the experimental joint cartesian coordinates $x_{exp,n}(t_k)$. The reason is that the approach is based on a multibody model, composed of rigid bodies, for which a variable size of the bodies would be irrelevant.

2. The model joint cartesian coordinates $x_{mod,n}$ are given by a forward kinematic model using the l_i distances and an initial value (set to zero) of the joint coordinates $q(t_k)$ that we want to determine. The cost function of this least-square optimization is defined as the sum of the square components of the absolute error vector between $x_{exp,n}(t_k)$ and $x_{mod,n}(q(t_k))$ of the n optokinetic sensors at the time instant t_k. In order to improve the process convergence, the optimal value of $x_{mod,n}(q(t_k))$ becomes the initial condition of the next iteration at the time instant t_{k+1}.
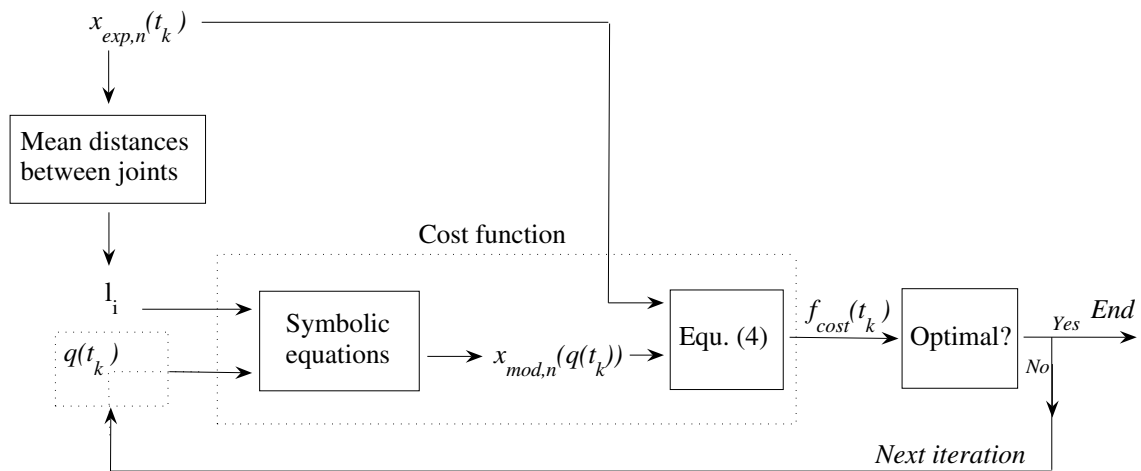
Figure 4. Identification process for a body configuration, at a time instant t_k, as proposed by Ref. [20].

The corresponding velocities $\dot{q}$ and accelerations $\ddot{q}$ are presently derived from the joint coordinates $q(t_k)$ and approximated by finite differences. The noise in $q(t_k)$ could be a significant source of error in the $\dot{q}$ and $\ddot{q}$ estimations, and thus in the dynamical analysis. Consequently, an optimization of $\dot{q}$ and $\ddot{q}$ will probably be suggested in the future. Nevertheless, the fact that the $x_{exp,n}$ are measured using an adaptive low-pass numerical filter and that the $q(t_k)$ are obtained using a kinematic optimization largely improves the $\dot{q}$ and $\ddot{q}$ accuracy.

2.4.2. Dynamical analysis

As proposed by Ref. [39], the system dynamical equations are obtained from a Newton-Euler formalism [26, 27]: this algorithm provides the vector Q of internal interaction torques and forces at the joints for any configuration of the multibody system, in the form of an inverse dynamical model (Equation 5), a semi-direct dynamical model (Equation 6) :

$$Q = f(q, \dot{q}, \ddot{q}, F_{ext}, M_{ext}, g) \tag{5}$$
$$= M(q)\ddot{q} + G(q, \dot{q}, F_{ext}, M_{ext}, g) \tag{6}$$

where

- q (42×1) is the vector of the human body joint coordinates, i.e. successively the three angular coordinates for each of the 13 members (*3 (translations for the first member LCOM position) + 13 (members) × 3 (angular coordinates) = 42 components*); the three angular coordinates per member represent the spherical joint; let us note that three translations per joint have been introduced and locked in order to permit the joint force calculations without interfering with the model [26, 27];

- $\dot{q}$ and $\ddot{q}$ (42×1) are the joint velocities and accelerations, respectively;

- F_{ext} and M_{ext} (42×1) are the three-dimensional components of the global external forces and torques applied to each of the body members;

- g (1×3) is the gravity;

- $M(q)$ (42×42) is the positive-definite symmetric mass matrix;
- $G(q, \dot{q}, F_{ext}, M_{ext}, g)$ (42×1) is the dynamical vector containing the gyroscopic, centrifuged and three-dimensional terms resulting from the system configurations, velocities, and also the external forces and torques and gravity applied to the system.

3. Results

In this section, the model is applied to two behaviors of STS, as follows :

- At each time instant t_k, the kinematic optimization problem provides the human body joint coordinates $q(t_k)$ that best fit the experimental joint positions $x_{exp,n}(t_k)$. From these results, a error analysis of the fitted model and a short joint kinematic analysis are developed for two behaviors of STS, defined as a *slow* and a *fast* motion, respectively.
- The inverse dynamical model provides the vector Q of the joint forces and torques for the slow and fast motions, respectively.

Furthermore, segment animations have been developed in order to present the kinematics and dynamics results on the model in a convenient manner. These animations are available on Ref. [40], and a few samples are described in this section.

3.1. Kinematic analysis

In terms of CPU time performance, the kinematic identification process, using $MATLAB^{TM}$ on a Pentium IV 530, 3 GHz processor, requires ca. 30 CPU seconds per 100 experimental samples, i.e. per second of studied motion. Further, the data reconstruction for the animation requires ca. 25 CPU seconds per second of studied motion. Consequently, the total optimization and display process requires ca. 55 CPU seconds per second of studied motion, i.e. in practice, this approximately requires 11 minutes for 10 seconds of motion data recording. Finally, let us note that the identification process time was reduced by 60% using a *mexfunction* from $MATLAB^{TM}$ to C++.

At each time instant t_k, the model joint cartesian coordinates $x_{mod,n}(q(t_k))$ of one behavior (here, the fast motion) can be recalculated in order to build the fitted model (blue in Fig. 5). This fitted model, using purely rigid bodies, can be compared to the purely experimental model (red in Fig. 5), based on the experimental joint cartesian coordinates $x_{exp,n}(t_k)$.

Further, an error analysis provides the global relative errors between $x_{mod,n}(q(t_k))$ and $x_{exp,n}(t_k)$ for the two behaviors of STS, in percentage of the corresponding $x_{exp,n}(t_k)$ at each time instant t_k (Fig. 6). For the fast motion (resp. the low motion), the maximal value of the global relative error is equal to 11.46% (resp. 8.27%) of the corresponding $x_{exp,n}(t_k)$, and the mean value of the global relative error is equal to 0.31% (resp. 0.33%), corresponding to a mean absolute error equivalent to 3.8mm (resp. 3.9mm) in each direction at each joint. In both cases, the error peaks occur during the transient phase of the motion.

Finally, selected results of joint kinematics are presented as follows :

1. The GCOM trajectories are presented (Fig. 7) during the slow a fast motions.
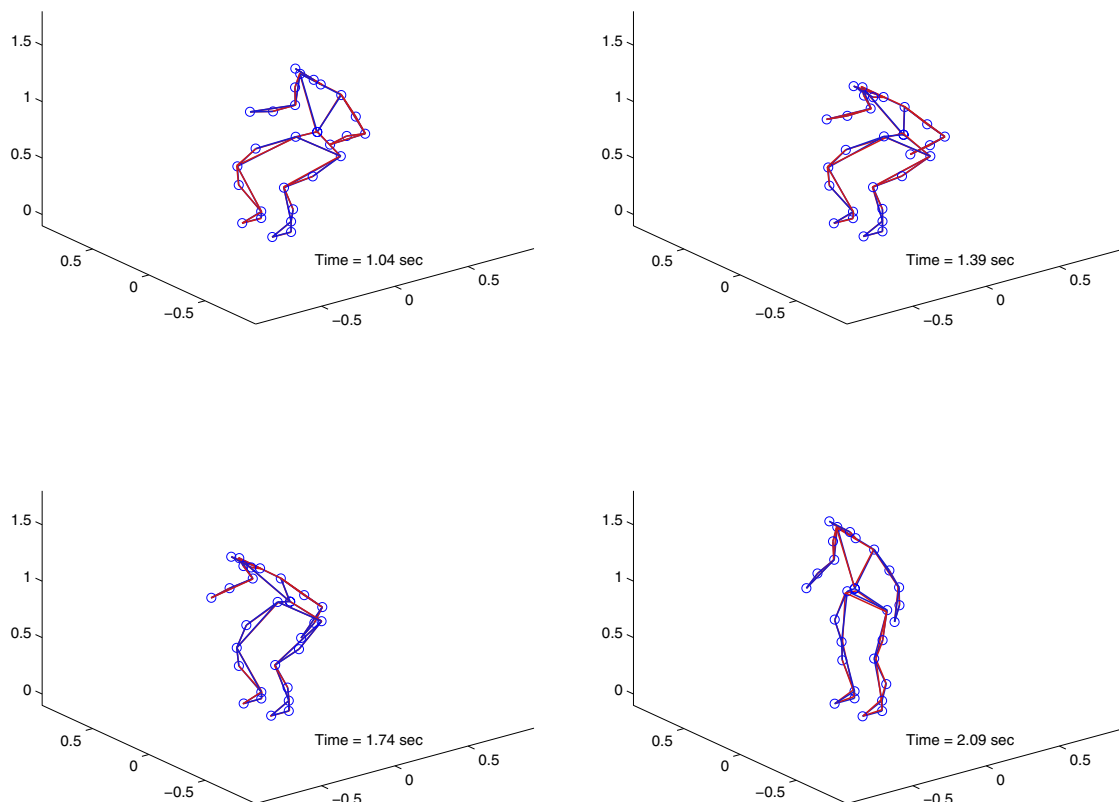
Figure 5. Fast STS: kinematic fit for four time instant t_k; superimposition of the fitted model coordinates $x_{exp,n}(t_k)$ (in blue) and the experimental model coordinates $x_{mod,n}(q(t_k))$ (in red).
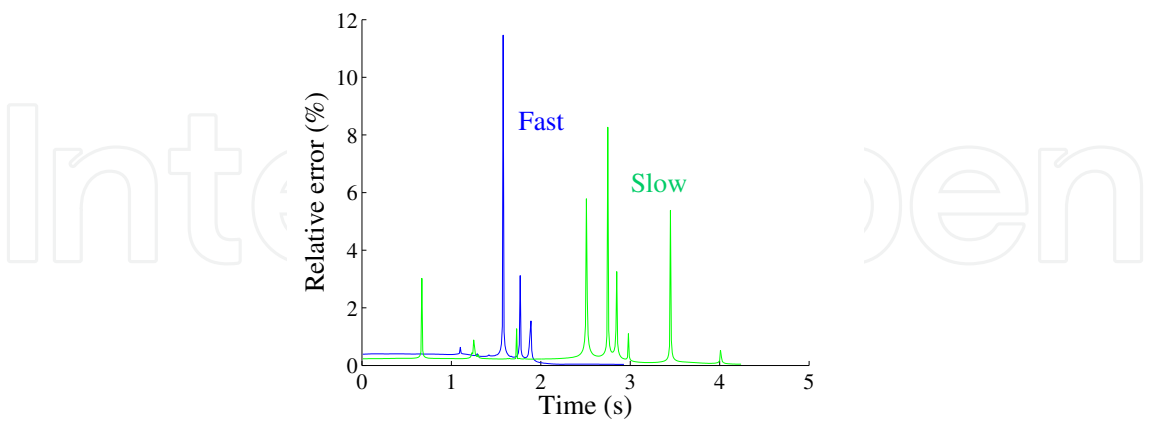

Figure 6. Error analysis: time evolution of the global relative error between $x_{mod,n}(q(t_k))$ and $x_{exp,n}(t_k)$, during the slow (green) and fast (blue) getting-up motions.

2. As an example, the model joint kinematics are compared during the slow a fast motions, for two joints : the consecutive angular coordinates R_3, R_1 and R_2 are described at the

sacrum (Fig. 8), i.e. from the pelvis member to the trunk member, and also at the right elbow (Fig. 9), i.e. from the upper arm to the lower arm.
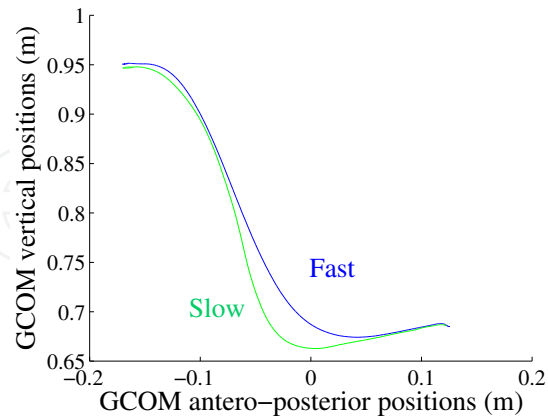

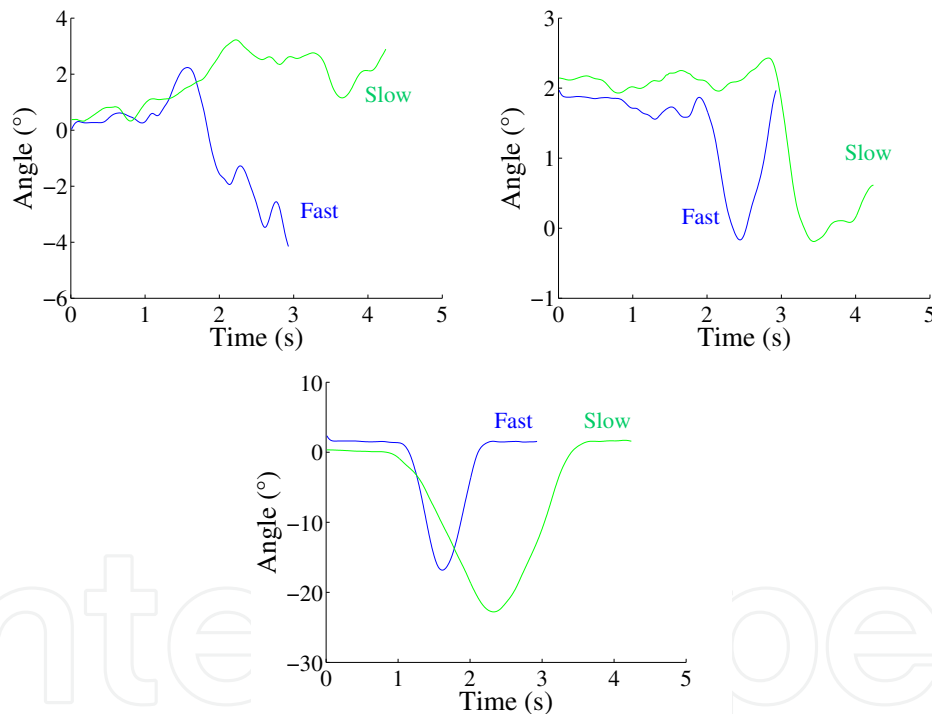**Figure 7.** Trajectory of the GCOM during the slow (green) and fast (blue) getting-up motions.

Figure 8. Time evolution of the three consecutive angular coordinates R_3, R_1 and R_2, respectively, at the sacrum: comparison of the slow (green) and fast (blue) getting-up motions.

3.2. Dynamical analysis

On the basis of the reference frame defined in Fig. 3, the dynamical analysis provides the time evolution of the global joint torques (Fig. 10) and forces (Fig. 11), for the slow and fast behaviors.
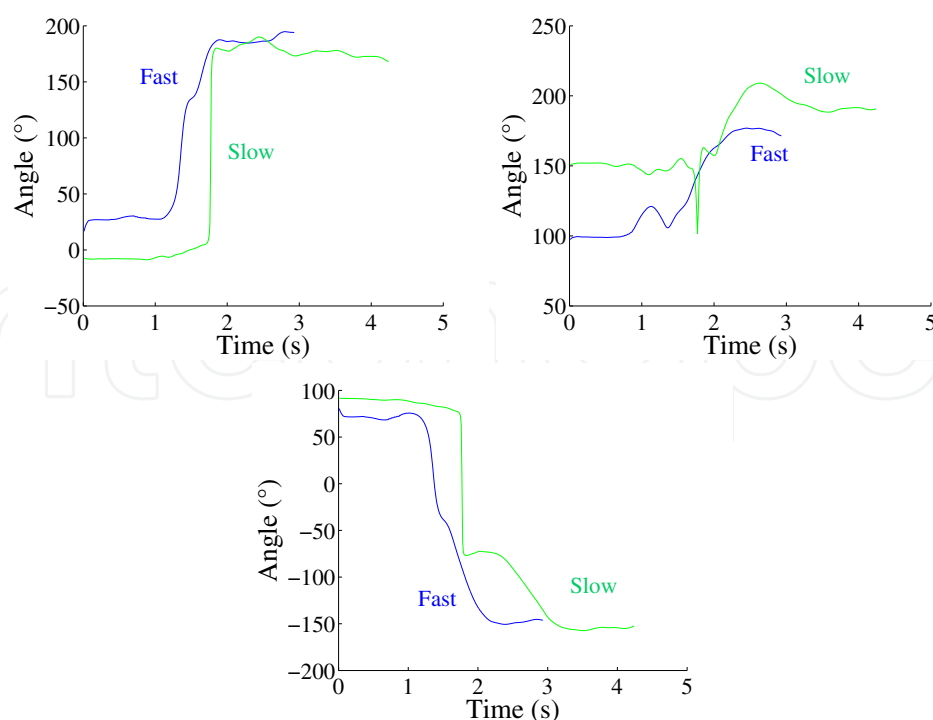
Figure 9. Time evolution of the three consecutive angular coordinates R_3, R_1 and R_2, respectively, at the elbow: comparison of the slow (green) and fast (blue) getting-up motions.

Furthermore, body segment animations have been developed in order to show the evolution of the joint positions, the corresponding global joint torques, and also the local and global centers of mass and pressure. Samples of this animation are presented in Fig. 12, at four time instants t_k during the fast STS behavior.

4. Discussion and conclusion

This section presents the benefits and limitations of this methodology, and also the perspectives for future studies.

4.1. Benefits and limitations

The present inverse dynamical model of the human body coupled with a kinematic identification of the model configurations (Fig. 1) is proposed as an accurate method to estimate the joint efforts in dynamical contexts, as presented from Fig. 1. Nevertheless, three main limitations of the present inverse dynamical model must be discussed.

1. *The geometrical limitation, due to the use of spherical joints :* The results of the kinematic analysis for this experiment show that the spherical joints considered here sufficiently fit the considered motion, with $x_{mod,n}(q(t_k))$ errors corresponding to a mean absolute error inferior to 3.9mm in each direction at each joint. However, using previous investigation results, the present model will be extended to include more involved joints in the future, particularly for the knees [34] and the shoulders [35].
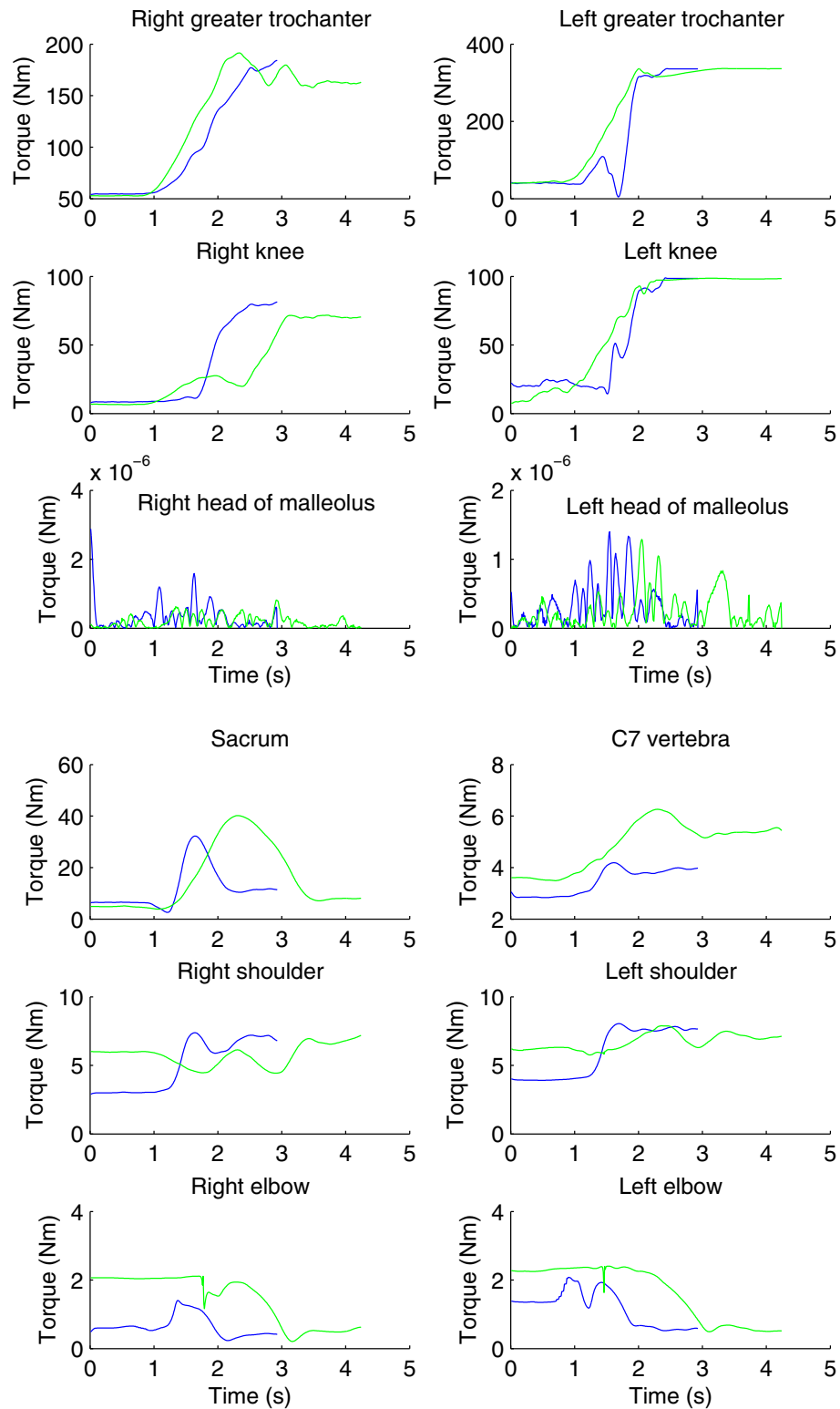
Figure 10. Time evolution of the global joint torques: superposition of the global joint torques at each joint, during the slow (green) and fast (blue) getting-up motions.
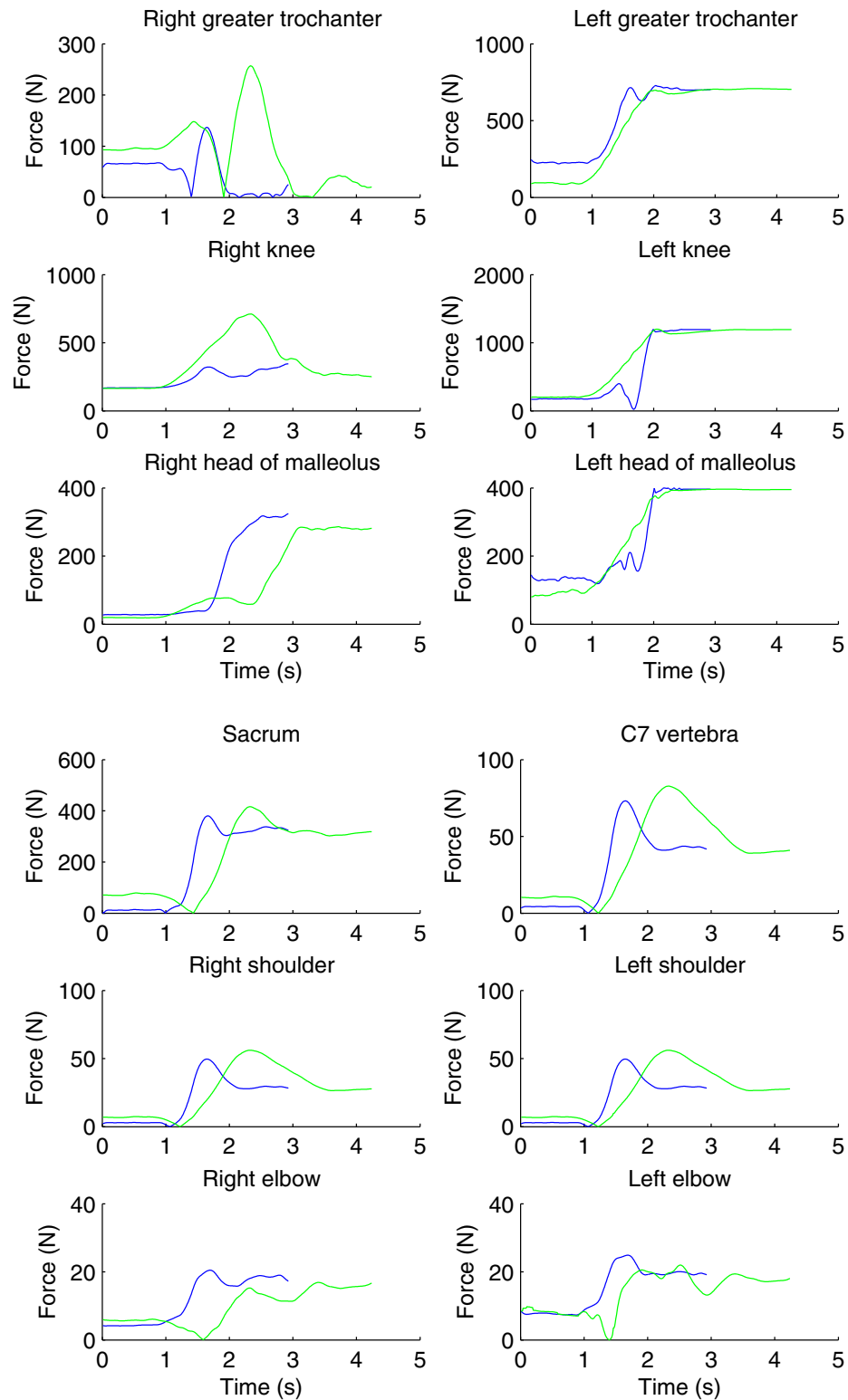
Figure 11. Time evolution of the joint forces: superposition of the three components of joint forces at each joint, during the slow (green) and fast (blue) getting-up motions.
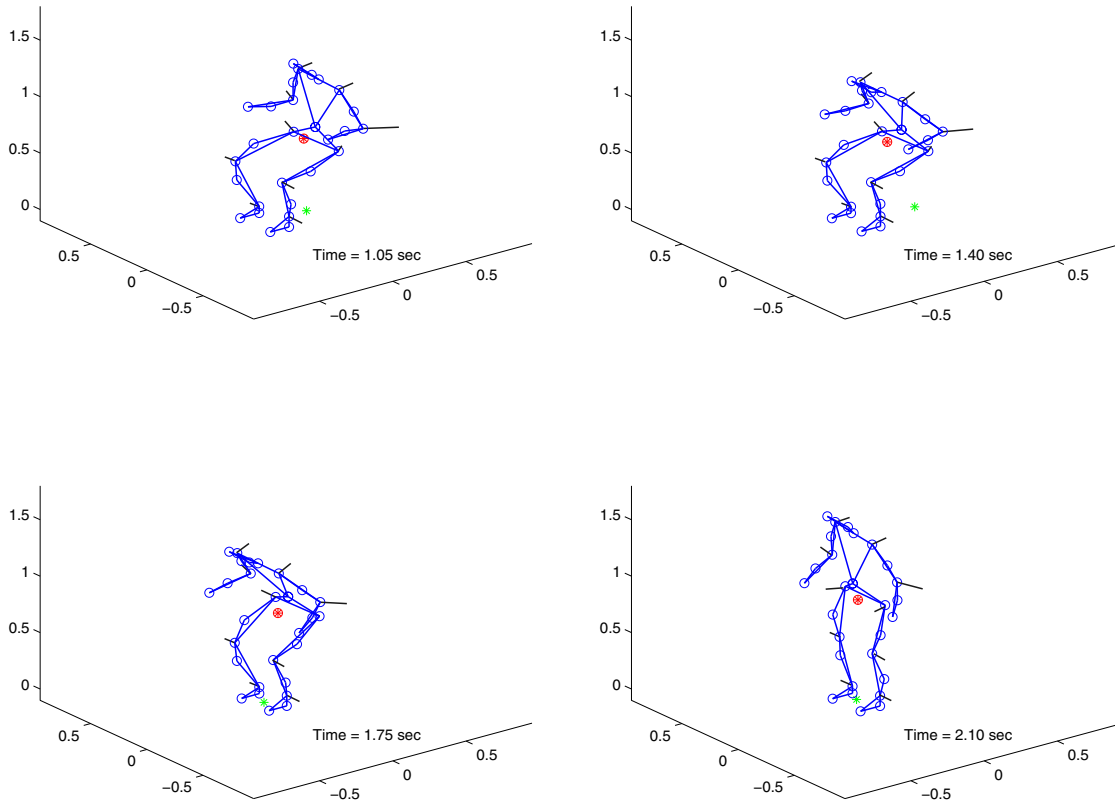
Figure 12. Samples of the fast STS, at four time instants t_k : the fitted model (in blue), featuring the global torques (in black) at each model joint, and also the GCOM (red point) and the GCOP (green star).

2. *The kinematic limitation, due to the rigid multibody system assumption :* Like other classical *dynamical inverse* analyzes [21–25] in biomechanics of motion, the proposed model is composed of linked rigid bodies. However, in reality, the body is not composed of a set of rigid bodies. Rather, each body member consists of a rigid part (bone), and a non-rigid part (skin, muscle, ligament, tendon, connective tissue, and other soft tissue structures) [38]: during any motion, the skeletal structures of the body experience accelerations, whereas the soft tissue motion is delayed, due to damped vibrations of the member. Consequently, the errors in the optimized joint coordinates q may introduce errors in the velocities $\dot{q}$ and accelerations $\ddot{q}$, and thus introduce errors in the estimation of the internal efforts.

3. *The dynamical limitation, due to the approximation of the body inertia parameters :* The body inertia parameters, i.e. the masses m_i, moments of inertia I_i and center of mass positions $\overrightarrow{OM_i}$ of the ith body member (i = 1,...,13) are approximated, using inertia tables [31]. Consequently, the errors in the estimated internal efforts Q increase if the corresponding body member accelerations increase. This is the reason why the present model is only proposed for rather small dynamics, such as the STS experiment, walking experiments or other motions without significant impact. Further, let us remember that previous investigations [33] showed that the non-invasive body parameter identifications during the

motions are presently inappropriate to the human body dynamics, because the resulting body parameters present large errors due to experimental errors in the input data, such as the body configuration, external force and torque measurements.

4.2. Perspectives

Finally, in the context of the hardness to perform efforts, the perspectives of this research is to quantify with a satisfying accuracy the main joint and muscle efforts of subjects in different dynamical contexts, and to apply the model to:

- physical therapy, in order to analyze joint efforts of subjects in different motion contexts, particularly for the evaluation, the follow-up and the treatment of patients in rehabilitation and orthopedics;
- comfort analysis is vehicle and car occupant dynamics, in order to analyze the hardness of going into and out of vehicles, and simulate the car occupant dynamics before crash.

Acknowledgements

Author details

Raison Maxime, Laitenberger Maria and Sarcher Aurélie
Research Chair in Pediatric Rehabilitation Engineering (CPRE), École Polytechnique de Montréal and CRME - Sainte-Justine UHC, Montreal, Canada

Detrembleur Christine
Institute of NeuroScience (IoNS), Université catholique de Louvain (UCL), Brussels, Belgium

Samin Jean-Claude and Fisette Paul
Centre for Research in Mechatronics (CEREM), Institute of Mechanics, Materials, and Civil Engineering (iMMC), Université catholique de Louvain (UCL), Louvain-la-Neuve, Belgium

5. References

[1] Bohannon RW (2011) Test-retest reliability of the five-repetition sit-to-stand test: a systematic review of the literature involving adults. J Strength Cond Res 25(11): 3205-7.

[2] Dos Santos AN, Pavão SL, Rocha NA (2011) Sit-to-stand movement in children with cerebral palsy: a critical review. Res Dev Disabil 32(6): 2243-52.

[3] Wang TH, Liao HF, Peng YC (2011) Reliability and validity of the five-repetition sit-to-stand test for children with cerebral palsy. Clin Rehabil. Epub ahead of print.

[4] Duncan RP, Leddy AL, Earhart GM (2011) Five times sit-to-stand test performance in Parkinson's disease. Arch Phys Med Rehabil 92(9): 1431-6.

[5] Jovic J, Fraisse P, Coste CA, Bonnet V, Fattal C (2011) Improving valid and deficient body segment coordination to improve FES-assisted sit-to-stand in paraplegic subjects. IEEE Int Conf Rehabil Robot. Jun 29 - Jul 1.

[6] Wetzel JL, Fry DK, Pfalzer LA (2011) Six-minute walk test for persons with mild or moderate disability from multiple sclerosis: performance and explanatory factors. Physiother Can 63(2): 166-80.

[7] Gao F, Zhang F, Huang H (2011) Investigation of sit-to-stand and stand-to-sit in an above knee amputee. Conf Proc IEEE Eng Med Biol Soc: 7340-3.

[8] Agrawal V, Gailey R, Gaunaurd I, Gailey R 3rd, O'Toole C (2011) Weight distribution symmetry during the sit-to-stand movement of unilateral transtibial amputees. Ergonomics 54(7): 656-64.

[9] Noguchi H, Hoshiyama M, Tagawa Y (2012) Kinematic analysis of sit to stand by persons with rheumatoid arthritis supported by a service dog. Disabil Rehabil Assist Technol 7(1): 45-54.

[10] Turcot K, Armand S, Fritschy D, Hoffmeyer P, Suvà D (2012) Sit-to-stand alterations in advanced knee osteoarthritis. Gait Posture. Epub ahead of print.

[11] Boyne P, Israel S, Dunning K (2011) Speed-dependent body weight supported sit-to-stand training in chronic stroke: a case series. J Neurol Phys Ther 35(4): 178-84.

[12] Kim I, Cho W, Yuk G, Yang H, Jo BR, Min BH (2011) Kinematic analysis of sit-to-stand assistive device for the elderly and disabled. IEEE Int Conf Rehabil Robot. Jun 29 - Jul 1.

[13] Jun HG, Chang YY, Dan BJ, Jo BR, Min BH, Yang H, Song WK, Kim J (2011) Walking and sit-to-stand support system for elderly and disabled. IEEE Int Conf Rehabil Robot. Jun 29 - Jul 1.

[14] Kinoshita S (2012) Handrail position and shape that best facilitate sit-to-stand movement. J Back Musculoskelet Rehabil 25(1): 33-45.

[15] Silva M, J Ambrósio, Pereira M (1997) A multibody approach to the vehicle and occupant integrated simulation. International Journal of Crashworthiness 2(1): 73-90.

[16] Pérez M, Ausejo S, Pargada J, Suescun A, Celigüeta JT (2003) Application of multibody system analysis for the evaluation of the driver's discomfort. Proceedings CD-rom of the multibody dynamics, July 1-4, Lisbon, Portugal.

[17] Bouisset S, Le Bozec S, Ribreau C (2002) Postural dynamics in maximal isometric ramp efforts. Biological Cybernetics 87(3): 211-19.

[18] Raison M, Detrembleur C, Fisette P, Willems PY (2004) Determination of joint efforts of a moving human body by inverse dynamics. Archives of Physiology and Biochemistry 112, suppl. September, 1-179: 90.

[19] Fujimoto M, Chou LS (2012) Dynamic balance control during sit-to-stand movement: an examination with the center of mass acceleration. J Biomech 45(3): 543-8.

[20] Raison M, Detrembleur C, Fisette P, Samin JC (2011) Assessment of Antagonistic Muscle Forces During Forearm Flexion/Extension. Multibody Dynamics: Computational Methods and Applications 23: 215-38.

[21] Denoth J, Gruber K, Ruder H, Keppler M (1984) Forces and torques during sport activities with high accelerations. Biomechanics current interdisciplinary research. Eds. Perren SM and Schneider E. Martinuis Nijhoff Pub. Dodrecht, Netherlands: 663-668.

[22] De Jalón G, Bayo E (1993) Kinematic and dynamic simulation of multibody systems: the real-time challenge. Springer, New-York: 440 p.

[23] Silva M, Ambrósio J, Pereira M (1997) Biomechanical Model with Joint Resistance for Impact Simulation. Multibody System Dynamics 1(1): 65-84.

[24] Silva M, Ambrósio J (2004) Sensitivity of the Results Produced by the Inverse Dynamic Analysis of a Human Stride to Perturbed Input Data. Gait and Posture 19(1): 35-49.

[25] Zacher I (2004) Strength Based Discomfort Model of Posture and Movement. SAE International Digital Human Modelling Conference, June 15-17, Rochester, Michigan.

[26] Fisette P, Postiau T, Sass L, Samin JC (2002) Fully symbolic generation of complex multibody models. Mechanics of Structures and Machines 30(1): 31-82.

[27] Samin JC, Fisette P (2003) Symbolic Modeling of Multibody Systems, Kluwer Academic Publisher: 484 p.

[28] Detrembleur C, Van Den Hecke A, Dierick F (2000) Motion of the body centre of gravity as a summary indicator of the mechanics of human pathological gait. Gait and Posture 12: 243-50.

[29] Bouisset S, Maton B (1996) Muscles, Posture et Mouvement. Herman Edition, Paris, 735 p.

[30] Bouisset S (2002) Biomécanique et physiologie du mouvement. Abrégés, Editions Masson: 304 p.

[31] De Leva P (1996) Adjustments to zatsiorsky-seluyanov's segment inertia parameters. Journal of Biomechanics 29(9): 1223-30.

[32] Zatsiorsky VM, Seluyanov VN, Chugunova L (1990) In vivo body segment inertial parameters determination using a gamma-scanner method. Biomechanics of human movement: Applications in rehabilitation, sports and ergonomics; edited by Berme N and A Cappozzo: 187-202.

[33] Chenut X, Fisette P, Samin JC (2002) Recursive Formalism with a Minimal Dynamic Parametrization for the Identification and Simulation of Multibody Systems. Application to the Human Body. Multibody System Dynamics 8: 117-40.

[34] Bao H, Willems PY (1999) On the kinematic modelling and the parameter estimation of the human knee joint. Journal of Biomechanical Engineering 121: 406-13.

[35] Bao H, Willems PY (1999) On the kinematic modelling and the parameter estimation of the human shoulder. Journal of Biomechanics 32: 943-50.

[36] Heglund N (1981) A simple design for a force-plate to measure ground reaction forces. Journal of Experimental Biology 93: 333-38.

[37] Eames MHA, Cosgrove A, Baker R (1998) A Full body model to determine the total body centre of mass during the gait cycle in adults and children. Fifth International Symposium on the 3-D Analysis of Human Movement, Chattanooga, Tennessee, USA, July 2-5.

[38] Nigg BM, Herzog W (1999) Biomechanics of the musculo-skeletal system. Eds. Nigg BM and W Herzog. 2d edition. Chichester and New York. 644 p.

[39] Raison M, Aubin CE, Detrembleur C, Fisette P, Mahaudens P, Samin JC (2010) Quantification of intervertebral efforts during gait: comparison between subjects with different scoliosis severities. Studies in Health Technology and Informatics 158: 107-11.

[40] Raison M et al. Website of the Research Chair in Pediatric Rehabilitation Engineering, École Polytechnique de Montréal and CRME - Sainte-Justine UHC, Montreal, Canada. Available: www.groupes.polymtl.ca/cgrp. Accessed 2015 Apr 15.